Variation of Vertical Structure of Precipitation in Wet and Dry Spells during the Southwest and Northeast Monsoon Seasons over the Arabian Sea and Bay of Bengal

Master's Thesis
submitted to

Indian Institute of Science Education and Research Tirupati
in partial fulfillment of the requirements for the

BS-MS Dual Degree Programme

by

N. S. Chiranjeevi
Roll Number: 201501030

Supervisor: Dr. K. Saikranthi
Inspire faculty,
Department of Earth and Climate Science
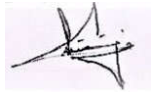Indian Institute of Science Education and Research, Tirupati

May, 2020

Certificate

This is to certify that the MS Thesis entitled "Variation of Vertical Structure of Precipitation in Wet and Dry Spells during the Southwest and Northeast Monsoon Seasons over the Arabian Sea and Bay of Bengal", submitted towards the partial fulfillment of the BS-MS dual degree programme at the Indian Institute of Science Education and Research Tirupati, represents the study / work carried out by N. S. Chiranjeevi at Indian Institute of Science Education and Research, Tirupati under the supervision of Dr. K. Saikranthi, Department of Earth and Climate Science, during the academic year 2019-2020 and the same has not been submitted for any other degree or diploma of any other university or institute.

Name of student: N. S. Chiranjeevi

Roll Number: 201501030

Signature of student:

Date: 15/05/2020

Name of Supervisor: Dr. K. Saikranthi

Signature of Supervisor:

Date: 15/05/2020

Declaration

I declare that the matter presented in the MS thesis entitled "Variation of Vertical Structure of Precipitation in Wet and Dry Spells during the Southwest and Northeast Monsoon Seasons over the Arabian Sea and Bay of Bengal", are the results of the work carried out by me at the Department of Physics, Indian Institute of Science Education and Research Tirupati under the supervision of Dr. K. Saikranthi.
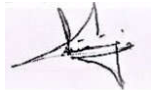
The contents are expressed in my own words and where others ideas have been included, I have adequately cited and referenced the original sources. I also declare that I have adhered to all principles of academic ethics and integrity and have not fabricated or falsified any idea / data / fact / image source in my submission.

I understand that violation of the above will lead to disciplinary action by the Institute and can also evoke penal action from the sources which have thus not been properly cited or from whom proper permission has not been obtained.

Name of student: N. S. Chiranjeevi

Roll Number: 201501030

Signature of student:

Date: 15/05/2020

Endorsed by

Name of Supervisor: Dr. K. Saikranthi

Signature of Supervisor:

Date: 15/05/2020

Acknowledgements

List of Publications

1. Variation of Vertical Structure of Precipitation in Wet and Dry Spells during the Southwest and Northeast Monsoon Seasons over the Arabian Sea and Bay of Bengal

   Authors: Saikranthi Kadiri, Chiranjeevi N S

   Submitted on 05 Mar 2020 to the Journal of Atmospheric Research

   Manuscript number: ATMOSRES_2020_307

Abstract

The characteristics of vertical structure of precipitation in wet and dry spells over the Arabian Sea (AS) and Bay of Bengal (BOB) during southwest monsoon (SWM) and northeast monsoon (NEM) seasons are elucidated using 16 years (1998-2013) of tropical rainfall measurement mission (TRMM) version # 7 2A25 and 3B42 datasets. The characteristics of precipitation differ from wet to dry spells in a given season as well as from SWM to NEM. Regardless of the season, the wet spells consists of more number of deeper and less number of shallow systems than the dry spells. The changes in the occurrence and rain fraction of different kinds of precipitating systems are marginal during the wet spells in both the seasons and seas. The shallow systems are abundant in dry spells of AS during SWM and NEM, where the background atmospheric conditions show lower total column water vapor (TCWV), drier mid-troposphere, frequent stable layers in lower troposphere and strong downdrafts. These conditions retard the vertical growth of the systems, which precipitate in the form of shallow rain. However, in the dry spells of BOB, rain fraction and occurrence of stratiform and convective (deep wide convective) rain decreases and shallow rain increases from SWM to NEM. Consequently, a bimodal distribution is observed in the reflectivity and storm height distributions at 3 and 5.5 km. The drier mid-troposphere, frequent stable layers in lower troposphere, lesser TCWV and strong downdrafts are observed in NEM than in SWM, which results in higher occurrence of shallow systems than the deep systems during the NEM. The Monsoon rainfall has socio-economic impact in the country as extended spells can cause monsoonal floods or droughts in regions, which can severely affect crop yields. Both the monsoons are land, atmosphere and ocean coupling systems therefore studying the characteristics of the variations in rainfall over the Indian Ocean can help us better predict and assess the impact of these spells over land.

Contents

List of Figures

List of Tables

List of Symbols

Z_m	:	Radar reflectivity
σ^o	:	Path integrated attenuation
θ_e	:	Equivalent potential temperature
θ	:	Potential temperature
L_v	:	Latent heat of vaporization
w_s	:	Saturation mixing ratio
C_p	:	Specific heat at constant pressure
T	:	Absolute temperature
p_0	:	Standard pressure
r	:	Spatially averaged daily rainfall for a particular day in a given year
μ	:	Mean of average daily rainfall for all the years of a particular day
σ	:	Standard deviation of average daily rainfall for all the years of a particular day

List of Acronyms

AMSU	:	Advanced Microwave Sounding Unit
AS	:	Arabian Sea
BOB	:	Bay of Bengal
TRMM	:	Tropical Rainfall Measurement Mission
ASMR-E	:	Advanced Microwave Scanning Radiometer for Earth Observing Systems
BB	:	Bright Band
BSR	:	Broad Stratiform Regions
CFAD	:	Contour Frequency by Altitude Diagram
DCC	:	Deep Convective Cores
DWC	:	Deep Wide Convective Cores
ECMWF	:	European Centre for Medium-range Weather Forecasting
GPCC	:	Global Precipitation Climatology Centre
ISE	:	Isolated Shallow Echoes
JJAS	:	June July August September
NEM	:	Northeast Monsoon
OISST	:	Optimum Interpolation Sea Surface Temperature
OND	:	October November December
PIA	:	Path Integrated Attenuation
PR	:	Precipitation Radar
RH	:	Relative Humidity
SRA	:	Standardised Rainfall Anomaly
SSMI	:	Special Sensor Microwave Imager
SST	:	Sea Surface Temperature
SWM	:	Southwest Monsoon
TCI	:	TRMM Combined Instrument
TCWV	:	Total Column Water Vapour
TMI	:	TRMM Microwave Imager
VIRS	:	Visible Infrared Radiometer
WCC	:	Wide Convective Cores

Chapter 1

Introduction

1.1 Importance of Monsoons over India

1.2 Studies related to temporal variation of Monsoonal rainfall

1.3 Scope of the thesis

1.1 Importance of Monsoons over India
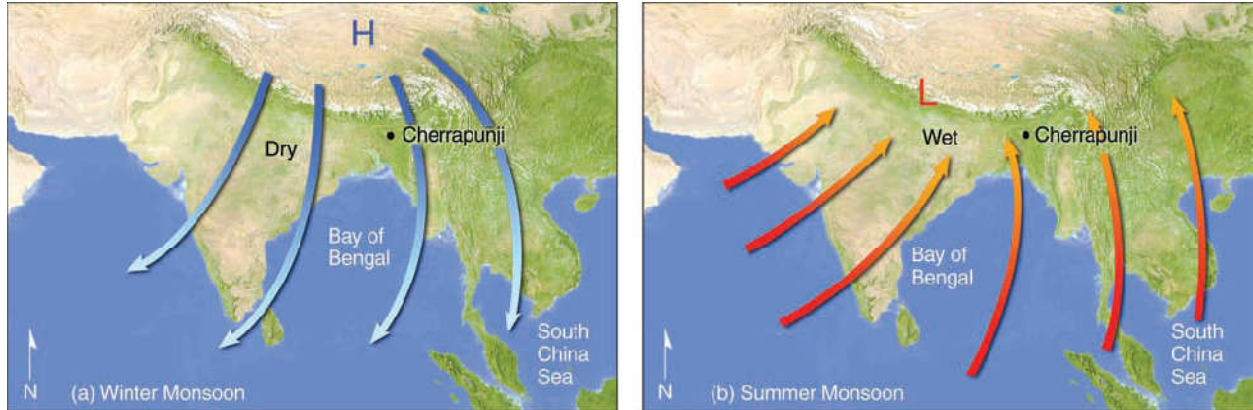
FIG. 1: (a) and (b) represents the NEM and SWM climatological wind patterns over Indian sub-continent respectively. (Ref. [41])

The word monsoon is originated from the Arabic word "Mausim" meaning seasons. The striking difference between continents and oceans in response to the solar energy received is responsible for monsoons. The term also technically describes seasonal reversals of wind direction caused by temperature differences between the land and sea breeze, creating zones of high and low pressure over land in different seasons (shown in FIG. 1). Southwest monsoon (SWM – June to September) and northeast monsoon (NEM – October to December) seasons over South Asia are considered as the world's most pronounced and unique weather phenomena [1]. The seasonal change in wind reversal during SWM and NEM are shown in Fig. 1. Most parts of Indian subcontinent receive 70-90% of their annual rainfall during the SWM. The NEM is also equally important especially over southern peninsular India, which receives 30-60% of its annual rainfall during this season [2]. Both these monsoons are land-atmosphere-ocean coupled systems, it is crucial to know the morphology of precipitation over the Arabian Sea (AS) and Bay of Bengal (BOB) along with the India landmass for their better representation in the climate models [3-5]. As the life and economy of India are vulnerable to changes in the monsoonal rainfall, it is of great interest inunderstanding and predicting the behaviour of monsoons dynamics and the variability of the rainfall at different temporal scales[6].

1.2 Studies related to temporal variation of Monsoonal rainfall

The monsoonal precipitating systems exhibit remarkable variations at intraseasonal, interannual and interdecadal time scales [6-8]. The intraseasonal oscillations play a vital role in modulating the seasonal and interannual rainfall variations [9] pronounced importance has been given to understand the monsoon intraseasonal variations.At intraseasonal time scales, the variations are classified into periods with excess rainfall known as wet spells and scanty rainfall denoted as dry spells. The low pressure systems, which are associated with higher rainfall, formed during the wet spells are seven times more than the dry spells. The duration of these spells vary from few days to more than a month. The rainfall during the monsoons shows three modes of oscillations (3-8 day; 10-20 day and 30-60 day) over the India [6, 10, 11]. The large temporal scale rainfall variations

are caused by changes in large-scale atmospheric and oceanic patterns, however in shorter time scales of 3-10 days are associated with synoptic scale activities. The rainfall variations with time scales of 30-60 days are termed as Madden Julian Oscillation.These oscillations are associated with large scale coupling between atmospheric circulation and tropical deep convection and demonstrates a northward and westward propagation of convective cloud bands from equatorial Indian Ocean [12-15]. The propagation direction of precipitating systems differs from one mode to other of oscillation over the equatorial Indian Ocean. For instance, the precipitating systems propagate towards north during the periods of 10-20 day oscillations and towards northwest during 30-60 day oscillations [12-16]. When compared with AS, the speed of propagation of rainfall is slower over BOB at the intraseasonal timescales [17]. The northward propagation from equatorial Indian Ocean is stronger and slower when central India experiences dry spell conditions and influences the consecutive wet spell near the equator [14].
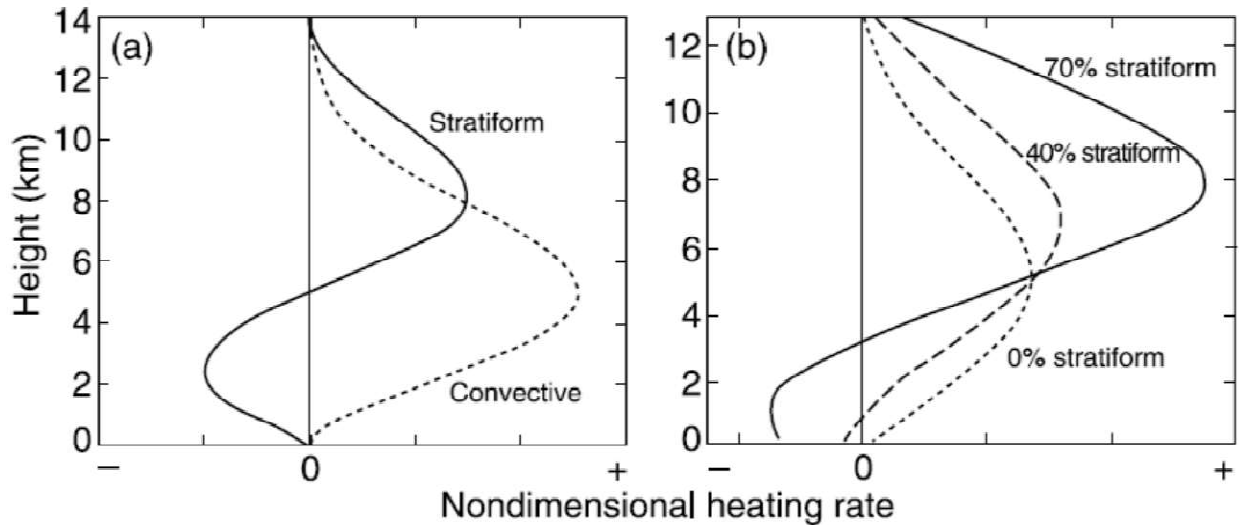
FIG. 2: (a) Idealized latent heat profiles for stratiform and convective precipitation in MCS. (b) Latent heat profiles by a mesoscale convective system with different stratiform rain fractions (Ref. [40]).

After the launch of the first precipitation radar (PR) onboard, the Tropical rainfall measuring mission (TRMM), a joint U.S.-Japan satellite mission to monitor tropical and subtropical precipitation, it gives an unique opportunity to study the rainfall characteristics over open oceans along with land mass. It observes a variety of variables that include radiances, microwave temperature, radar reflectivity, rainfall rate, vertical rainfall profile, and convective and stratiform heating. Using these observations, many recent studies have contributed significantly to the understanding of climatic phenomena that occurs over the tropics. Using the TRMM PR data and model outputs, [12] studied the role of convective and stratiform rain in altering the northward propagation. They showed that the convective rain exhibits weak northward propagation, while organized stratiform strongly modulates the northward propagation. They also emphasized the impact of latent heating at different heights during the stratiform rain on the northward propagation. Therefore, the information on stratiform and convective rain is vital for

simulating the northward propagation in the climate models during wet and dry spells [18] emphasized the importance of rain microphysical processes in simulating the accurate rainfall at intraseasonal timescales over Indian Ocean. The aforementioned studies on propagating systems over the Indian Ocean portray the need of understanding the characteristics of precipitating systems originated over the AS and BOB for better prediction of monsoonal rainfall over the India landmass.

The information on occurrence and vertical structure of various kinds of precipitating systems is crucial, as their interaction with the background atmosphere is distinctly different. For instance, the latent heating profile is distinctly different for different kinds of precipitation [19, 20] which in turn changes the thermal structure of the atmosphere. For example, for the stratiform rain, the net cooling is observed below the zero degree isotherm because of melting and evaporation of hydrometeors and because of condensation and vapor deposition the latent heat is released at all the heights above the zero degree isotherm. However, during the convective rain the latent heat is released at all the heights due to freezing and condensation. Hence with the change of occurrence of stratiform (or convective rain) the heating profile changes (Fig.2). In this connection using different datasets, numerous studies have reported the occurrence of different types of precipitation over India and its surrounded seas [10, 21-25]. Moreover, the spatial variation of different kinds of precipitating systems during El Niño and La Niña episodes and their association with the background atmospheric conditions over India and adjoining oceans are deliberated in [26]. Over open oceans sea surface temperature (SST) being the driving force for triggering the convection, its link with clouds [27], convection [28] and different types of rainfall [29] have been studied over the Indian Ocean during the SWM. In addition to the precipitating systems occurrence their vertical structure variation with SST has also been discussed in [29, 30].

1.3. Scope of the thesis:

All the aforementioned studies, dealt with understanding the seasonal differences of different kinds of precipitating systems i.e., in terms of their occurrence and vertical structure.However, the information on vertical structure and their association with the background atmosphere at intraseasonal time scales is less known over the AS and BOB, especially, during NEM it is least explored. Most of the studies considered AS and BOB as a single entity in the Indian Ocean to study the characteristics of rainfall. In reality, the wind patterns (Fig. 1), sea surface temperature (Fig. 3), atmospheric thermodynamic and dynamic variables are also different over both seas [29] during both the seasons. Hence in the present study the AS and BOB are considered are two different regions over Indian Ocean for studying the intraseasonal characteristics during SWM and NEM.
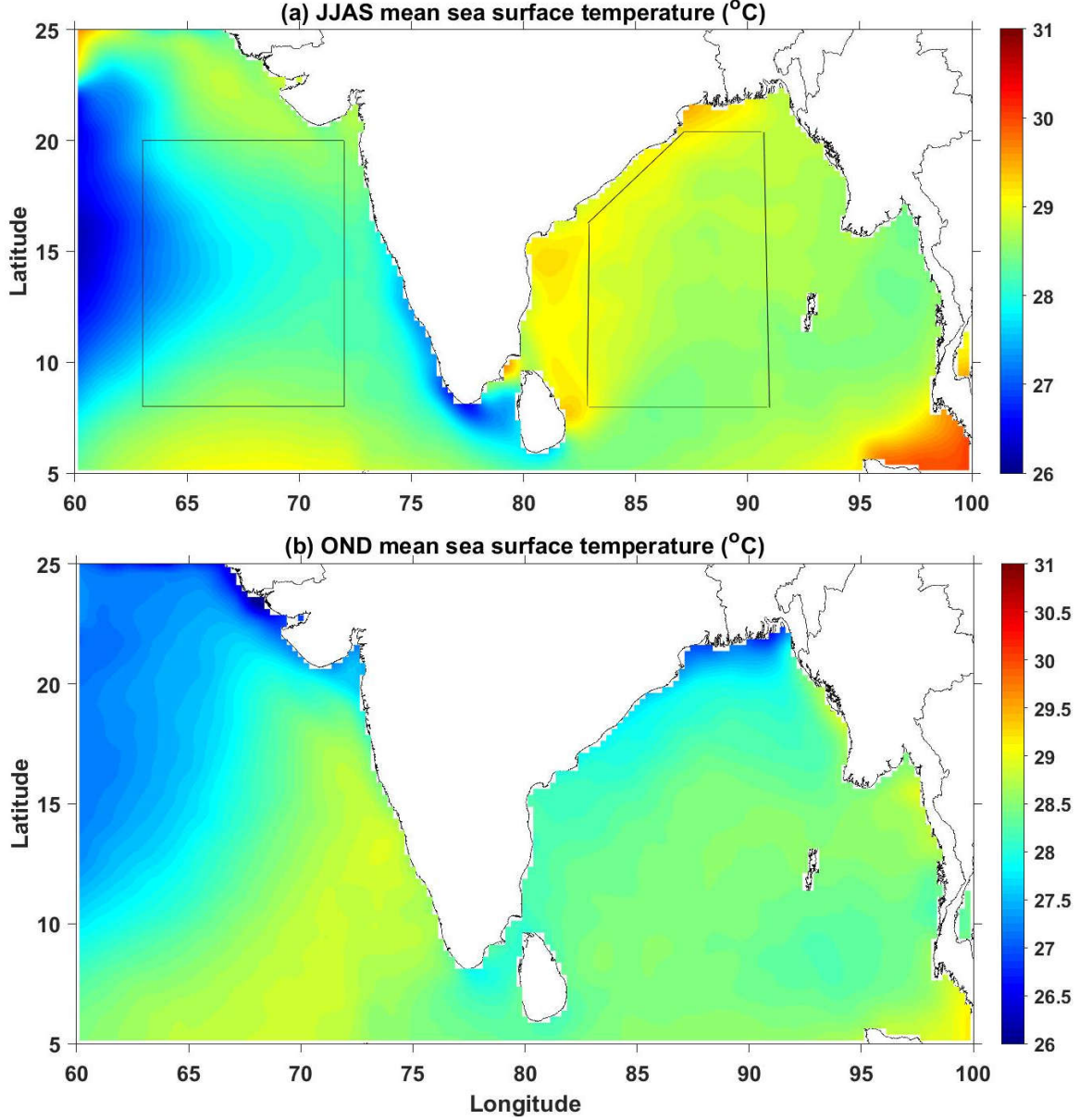
FIG. 3: (a) and (b) represents the mean sea surface temperature during 1998-2013 SWM and NEM respectively. The regions considered in the present study are shown as boxes in FIG. 1(a) covering the open oceans of AS (8–20° N, 63–72° E) and the BOB (8–21° N, 83–92° E) respectively.

Since SEM and NEM rainfall has socio-economic impact in the country, understanding and predicting the behavior of climatological monsoon dynamics at different temporal scales is highly essential to farmers and scientists. Even during normal rainfall years extended spells can cause monsoonal floods or droughts in regions because of uneven spatial and temporal rainfall distributions. This can severely impact crop yield as water is needed at specific periods and specific amounts of crop growth. Both the monsoons are land, atmosphere and ocean coupling systems, the knowledge of variation in the background atmospheric conditions, surface forcing along with the morphology of

precipitation over the Arabian Sea (AS) and Bay of Bengal (BOB) are important in order to understand the Indian monsoon. In this regard, the aim of the present thesis is to understand the following:

1.   The differences in occurrence of various rain types during wet and dry spells and also to understand the variations in the vertical structure of precipitation (in terms of vertical profiles of reflectivity and storm height) over the AS and BOB (both the regions are considered over open oceans are represented in Fig. 3) during the SWM and NEM.

2.   The association of variation of precipitating systems with the background atmospheric conditions prevailing over the two seas.

The results on this comprehensive study on the characteristics of precipitation during the intraseasonal timescale over AS and BOB and their associated background conditions are discussed in detail in chapter 4. The scope for the future work is also discussed in this chapter.

Chapter 2

Data and methodology

2.1 Tropical Rainfall Measuring Mission Precipitation Radar data (TRMM PR)

2.2 TRMM PR Algorithms

2.3 Off nadir beam issues related to TRMM PR data

2.4 Sensitivity, limitations of TRMM PR data

2.5 ECMWF reanalysis data (ERA 5)

2.6 Optimum interpolation sea surface temperature (OISST)

2.7 Identification of wet and dry spells

2.1. Tropical Rainfall Measuring Mission Precipitation Radar data (TRMM PR)
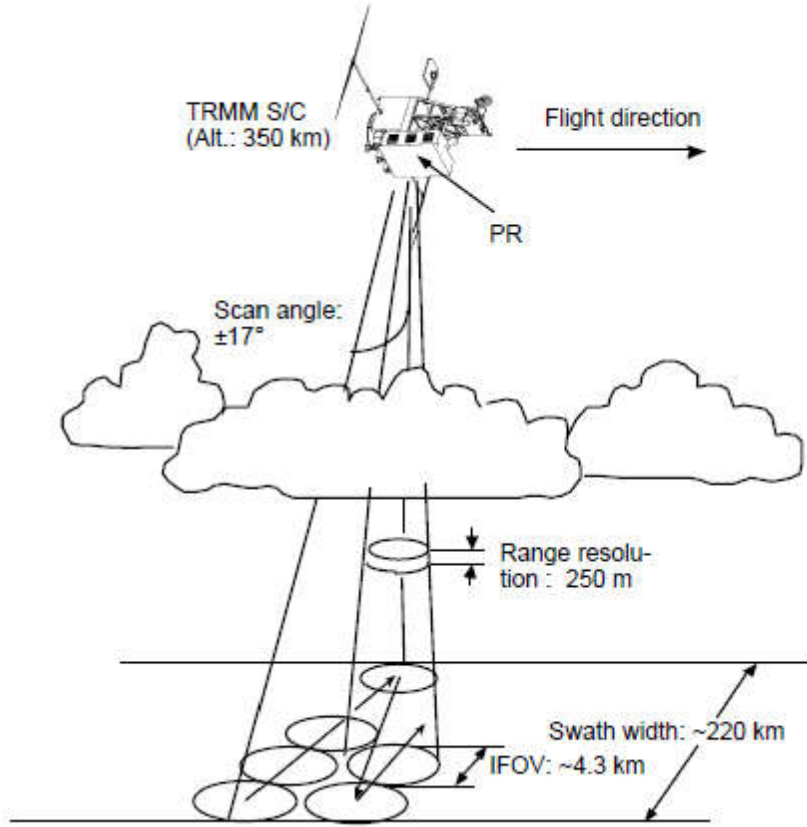
FIG. 4: A schematic diagram describing the scanning strategy of the Precipitation Radar onboard the TRMM (Ref. [42])

The data used in the project is obtained from The Tropical Rainfall Measuring Mission (TRMM). TRMM is a joint U.S.-Japan satellite mission to monitor tropical and subtropical precipitation. The TRMM PR is the first space borne precipitation radar. It directly observes vertical distributions of precipitation and gives us precipitation estimates over land and ocean as well as the three dimensional structure of rainfall information. The TRMM mission was active for 16 years (1998-2013) providing the wealth of three-dimensional climatological rainfall dataset over tropics. The TRMM satellite is composed of three main instruments to measure rainfall. The Visible Infrared Radiometer (VIRS) observes cloud coverage type and temperatures. The TRMM Microwave Imager (TMI) records the integrated column precipitation content rain intensity and type and other rainfall parameters. The scan strategy and the main parameters like frequencies, resolution etc of the TRMM PR are listed in FIG. 4 and Table 1.

Table 1: Main specifications of TRMM PR (Ref. [42])

Item	Specification
Frequency	13.796, 13.802 GHz
Sensitivity	$\leq \approx 0.7$ mm/h (S/N/pulse ≈ 0 dB)
Swath width	220 km (from end to end)
Observable Range	Surface to 15 km altitude
Horizontal resolution	4.3 km (nadir)
Vertical resolution	0.25 km (nadir)
Antenna	
Type	128-element WG Planar array
Beam width	0.71° x 0.71°
Aperture	2.0 m x 2. 0 m
Scan angle	$\pm$ 17° (Cross track scan)
Transmitter/receiver	
Type	SSPA & LNA (128 channels)
Peak power	$\geq$ 500 W (at antenna input)
Pulse width	1.6 μs x 2 ch. (Transmitted pulse)
PRF	2776 Hz
Dynamic range	$\geq$ 70 dB
Number of independent samples	64
Data rate	93.2 kbps
Mass	465 kg
Power	250 W

2.2 TRMM PR Algorithms

The radar algorithms used by the TRMM are classified into 3 levels (Level 1, Level 2 and Level 3) based on which stage of data processing they belong to. Each succeeding level uses outputs from the previous levels of processing. Level 1 algorithms include 1B21 calculates the Calibrated received power and 1C21 algorithm converts the received power into unattenuated radar reflectivity. Level 2 algorithms include 2A21, which gives us the path integrated attenuation of σ°, 2A23 algorithm detect the bright band and determine the rain type (convective, stratiform using the methods outlined by [31]), and the 2A25

algorithm calculates the attenuation-corrected radar reflectivity. There are also Level 3 product namely, 3A25 and 3A26, which calculate various statistics over a month from the Level 2 PR output products. Along with these level 3 products, 3B42 gridded data product derived by combining the data from multi satellites is available.

The multi satellite derived product 3B42 version 7 is used in the present study. The spatial extent of the data is divided into 1400x400 grids ($0 - 360°$E, $50°$N-$°$S) with a spatial resolution of $0.25°$ and a temporal resolution of 3 hours. The 3B42 algorithm used to get these precipitation estimates is as follows. The algorithm uses estimates from the TMI and a network of other satellites (ASMR-E, SSMI, AMSU and others) to detect precipitation. The first step in the calibration and combination of the microwave precipitation estimates to the TRMM Combined Instrument (TCI) estimates. This constitutes the TRMM product 3B31. From the calibrated microwave precipitation estimates the infrared precipitation estimates are created by using monthly matched microwave-IR histogram matching. The microwave and Infrared estimates are combined. This 3 hourly precipitation estimates are added to give us monthly estimates which are then combined with Global Precipitation Climatology Centre (GPCC) rain gauge analysis to give us the form a monthly best-estimate precipitation rate. This constitutes the TRMM product 3B43. The three hourly precipitation estimates for each grid box are then rescaled to match the monthly estimates. This constitutes the TRMM product 3B42. The TRMM Standard PR Algorithms, their nomenclature, products along with the brief description is mentioned in Table 2 and furthermore, the outline of standard algorithm flow chart for the TRMM PR is described in FIG. 5.
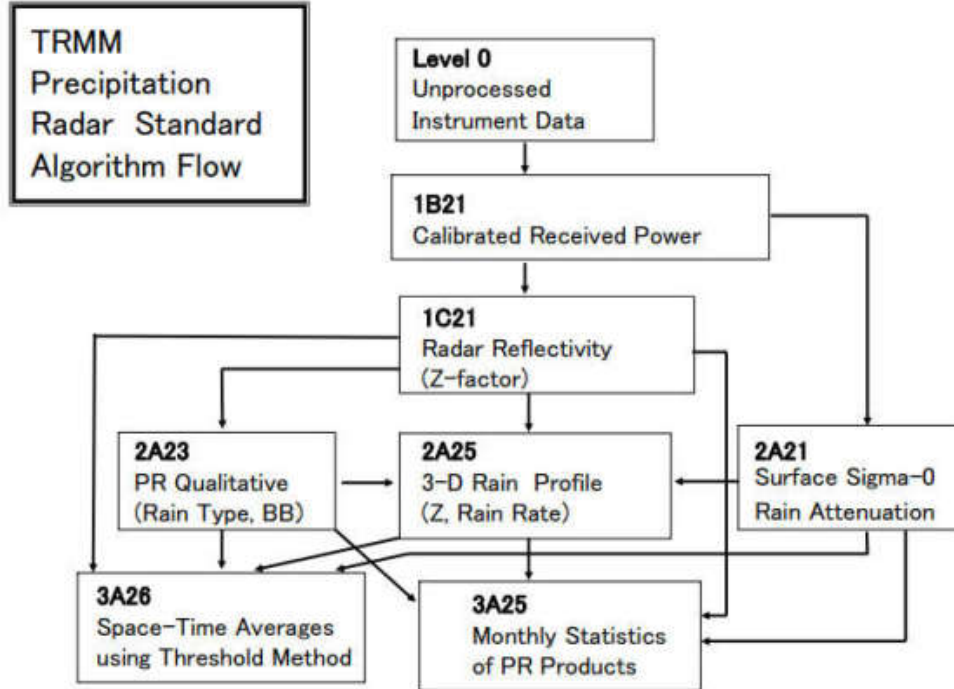
FIG. 5: The outline of standard algorithm flow chart for the TRMM PR data. (Ref. [42]).

Table 2: The following table outlines the TRMM Standard PR Algorithms, their nomenclature, products and a brief description. (Ref. [42])

Product No.	Name	Products	Algorithm Description
1B21	PR calibration rain/no rain	Total received power, noise level clutter contamination flag.	Conversion of the count value of radar echoes and noise level into engineering value. Decision of rain/no rain. Determination of effective storm height from minimum detectable power value. Rejection of mainlobe and sidelobe clutter.
1C21	PR reflectivities	Profiled Z_m (radar reflectivity factors without rain attenuation correction).	Conversion of the power and noise value to radar reflectivity factors Z_m without rain attenuation correction.
2A21	Surface scattering coefficient σ^o	Path integrated attenuation (PIA) of σ^o (in case of rain) and its reliability. Data base of σ^o (ocean/ and, in case of no rain)	Estimation of path integrated attenuation and its reliability using the surface as a reference target. Spatial and temporal statistics of surface σ^o and classification of σ^o into land/ocean, rain/no rain.
2A23	PR qualitative	Detection of bright band, Bright band height, strength, width, rain type classification, Detection of shallow isolated rain. Output of rain/no rain flag, height of storm top.	Whether a bright band exists in rain echoes or not, and determination of bright band height when it exists. The rain type is classified into stratiform type, convective type or others. Shallow isolated rain, the height of which is below the degree isotherm, is detected.
2A25	PR profile	Range profiles of attenuation-corrected radar reflectivity factors, rainfall rate. Estimated near surface, and surface rainfall rates, and average rainfall rates between the two predefined altitudes (2,4 km).	The rainfall rate estimate is given at each resolution cell. This algorithm employs a hybrid method of the surface reference method and the Hitschfeld-Bordan method. Precipitation water content at 5 altitudes, and vertically integrated precipitation water content are also calculated.

3A25	Space-time average of radar products	Space-time averages of accumulations of 1C21, 2A21, 2A23, 2A25.	Calculation of various statistics over a month from the level 2 PR output products. Four types of statistics are calculated. • probabilities of occurrence, • means and standard deviations, • histograms, • correlation coefficients.
3A26	Estimation of space-time rain rate statistics	Rain rate statistics over 5 degree x 5 degree 1 month space-time regions using a multiple thresholding technique.	Estimated values of the probability distribution function of the space-time rain rate at 4 levels, and the mean, standard deviation, and so on.
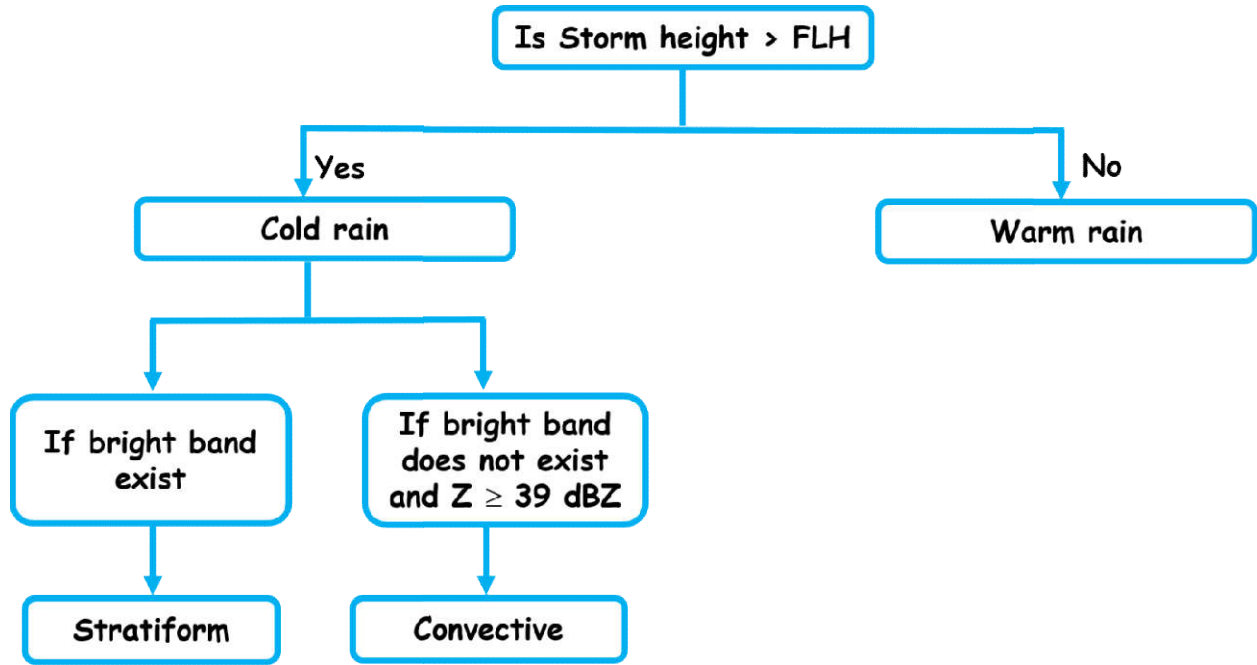
FIG. 6: The flowchart algorithm classification of different rain types by the Vertical profile method. FLH is the freezing level height and Z is reflectivity.

In the present study, the rain type classification is considered from the TRMM PR 2A23 radar algorithm described in [31]. There are two methods in which rain type is classified, namely the Vertical profile method (V method) and the Horizontal pattern method (H method). The TRMM PR uses a combination of these two methods for the rain type classification. In the V method the first step is to detect the presence of bright band (BB; height where the ice particles aloft melt to form raindrops), a region of high reflectivity (Z) at a certain height (below the zero degree isotherm). Further if the height

of the storm top (also called as storm height i.e., the topmost height at which the reflectivity is greater than the 17dBZ) is greater than freezing level height (FLH) it is classified as cold rain else it is classified as warm (or shallow) rain. If cold rain is detected and BB exist, it is classified as stratiform rain. If the BB does not exist and the maximum reflectivity value below the FLH is greater than or equal to a threshold value (39 dBZ) it is classified as convective rain. The schematic representation of V method is shown in FIG. 6. For the H method, the first step is to detect a convective core, a wide horizontal region of high reflectivity below the FLH. If the pixel is not detected as convective and BB is not certain and all the pixels surrounding it is detected as convective, then it is changed to convective in H method. If the region adjacent to the convective core is stratiform, the rain type is classified as stratiform and all the remaining pixels i.e., the radar echoes possibly from cloud or anvil are classified as 'other'. The classification results of the two methods are combined to give merged product described in Table 3.

Table 3: The table outlines the recombination of classification from the Vertical profile method (V method) and The Horizontal pattern method (H method)

V method	H method	Merged type
Stratiform	Stratiform	Stratiform
Stratiform	Other	Stratiform
Other	Stratiform	Stratiform
Stratiform (BB certain)	Convective	Stratiform
Convective	Convective	Convective
Other	Convective	Convective
Convective	Other	Convective
Convective	Stratiform	Convective
Stratiform (BB not so certain)	Convective	Convective
other	other	Other

2.3 Off nadir beam issues related to TRMM PR data
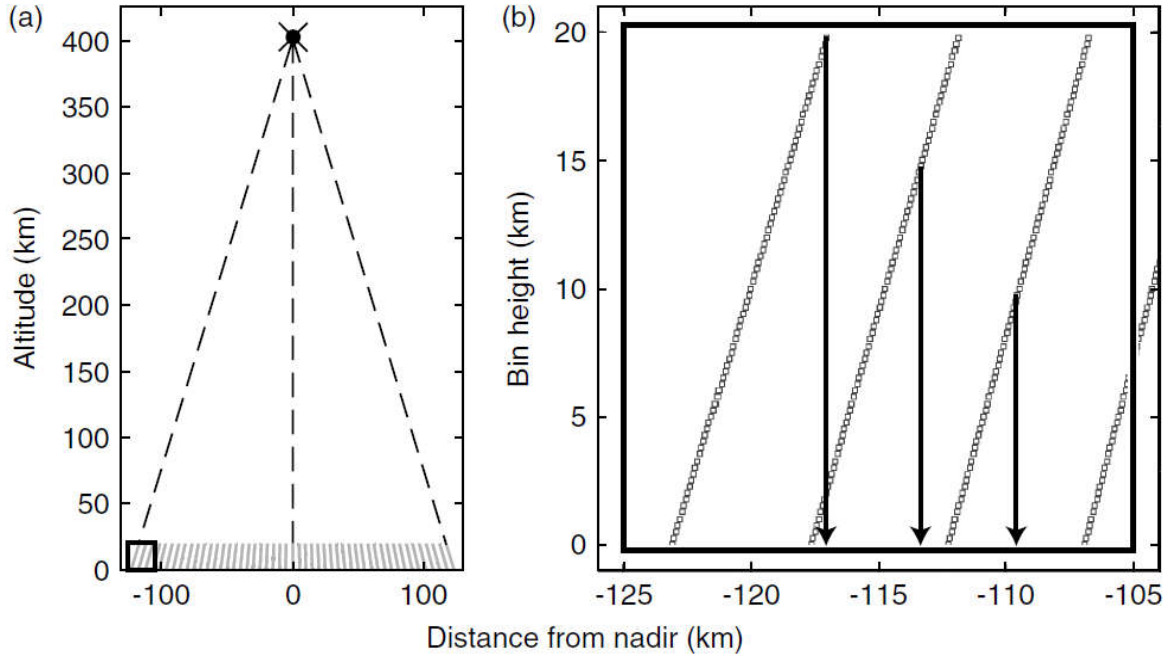
FIG. 7: (a) represents the scan geometry of TRMM PR from nadir to 17° scan width. (b) represents the expanded view of off nadir bins which is shown as box in FIG. 7a. The arrows shows the corrected reference point at each off nadir bin and the line with symbol 'o' represents its deviation of beam from straight path.

The geometry of TRMM PR scan angle from nadir to 17° scan width on both sides along with 49 angle bins (with 0.71° beam width) and 80 vertical levels are shown at the bottom of the FIG. 7a. The expanded view of the off nadir bins geometry is shown in FIG.. 7b. It clearly shows the deviation of scan geometry from the straight-line path to slant path (shown with symbol 'o' at each height in Fig. 7b). This deviation increases with increase in the scan angle towards the off nadir beams. The correction in 2A25 data (attenuation corrected reflectivity vertical profiles) regarding the geometrical issues in the off nadir beam is done by [32] (data is available at http://trmm.atmos.washington.edu/). Arrows in FIG. 5b show the corrected reference point. This correction is done by three-dimensional interpolation of TRMM PR data and the detailed procedure of interpolation is described in [32]. The spatial resolution of this data is 0.05° with 80 vertical levels from surface to 20km separated by 0.25km. Based on the horizontal and vertical extent of precipitation [32] further classified these profiles into deep convective cores (DCC), deep wide convective cores (DWC), wide convective cores (WCC), broad stratiform regions (BSR) and isolated shallow echoes (ISE). In the present study the systems identified using moderate thresholds are used i.e., DCC - intensity ≥ 30dBZ & storm height ≥ 8km, WCC - intensity ≥ 30dBZ & horizontal contiguous area ≥ 800 km^2, DWC are echoes satisfying

both DCC and WCC thresholds, BSR - 2A23 stratiform contiguous area $\geq$ 40,000 km^2, ISE - storm height $\leq$ freezing level height by at least 1km.

2.4 Sensitivity, limitations of TRMM PR data:

The sensitivity of the TRMM PR i.e., the minimum detectable radar echo is ~17dBZ and therefore cannot detect very lightest rainfall rates below 0.5 mm/hr. The limitation of TRMM PR is it gives only the data during overpass and hence the continous three-dimensional data cannot be obtained at a particular location. However, this data is highly useful and wealth worth to study the statistical three dimensional rainfall characteristics at a particular location with long-term dataset.

2.5 ECMWF reanalysis data (ERA 5):

To study the background conditions that existed over the seas during Wet and Dry spells we used the ERA5 Reanalysis data. ERA5 is a successor of ERA-Interim reanalysis dataset and is the fifth generation reanalyses dataset from the European centre for medium-range weather forecasting (ECMWF, Copernicus Climate Change Service (C3S) 2017). Analysis refers to the principle of data assimilation, which combines forecasts from numerical weather predictions centers with the latest recorded observations (every few hours) to give better estimates for better predictions. It gives us the atmospheric conditions in either a surface or single level or in multiple pressure levels (up to 37 levels).

It has a spatial resolution of 0.25° (further, it is regridded to 1° resolution is used in the present study) and a temporal resolution of 1 hour. The variables from ERA5 used in this study include total column water vapour, temperature, relative humidity, and vertical wind velocity. A negative value in vertical velocity indicates updraft and a positive value indicates a downdraft. To know the stability of atmosphere, equivalent potential temperature ($\boldsymbol{\theta}_e$), is calculated using the formula given in Wallace and Hobbs (2006):

$$\theta_e = \theta \frac{L_v w_s}{C_p T}$$

Where, $\boldsymbol{\theta}$, L_v, w_s, C_p and T represent the potential temperature, latent heat of vaporization, saturation mixing ratio, specific heat at constant pressure and absolute temperature, respectively.

2.6 Optimum Interpolation sea surface temperature (OISST)

To study the variation of sea surface temperature over AS and BOB during SWM and NEM from 1998 to 2013 the daily optimum interpolation sea surface temperature (OISST) data are used in the present study. This is a data product constructed by combining observations from different platforms (satellites, ships, buoys) on a regular global grid and the gaps are filled by interpolating the data [35]. It has a spatial resolution of 0.25° x 0.25° and a temporal resolution of 1 day.

2.7 Identification of wet and dry spells

In the present study to identify the wet and dry spells the 3B42 three hourly rainfall data are considered for the regions covering the open oceans over AS (63-72°E and 8-20°N) and BOB (83-92°E and 8-21°N). The daily rainfall estimates are calculated for the each grid and later the daily average regional rainfall is calculated for the two regions during SWM and NEM for all the years. Further using the daily rainfall the wet and dry spells are identified for AS and BOB for the two seasons following [36-38]. Firstly, the standardized rainfall anomaly for each day has been calculated using the formula given below:

$$Standardised\ rainfall\ anomaly\ (SRA) = \frac{r - \mu}{\sigma}$$

Where, SRA represents standardised rainfall anomaly, r be the spatially averaged daily rainfall for a particular day in a given year, μ indicates the mean of average daily rainfall for all the years of a particular day and σ represents the standard deviation of average daily rainfall for all the years of a particular day. If the SRA for each day is > 0.5 (< 0.5) for at least three consecutive days, then it is classified as a wet (dry) spell following [36-38]. In addition to these days, consecutive days having SRA > 0.25 or SRA < - 0.25 in the mid of the spell are added to wet and dry spells, respectively.
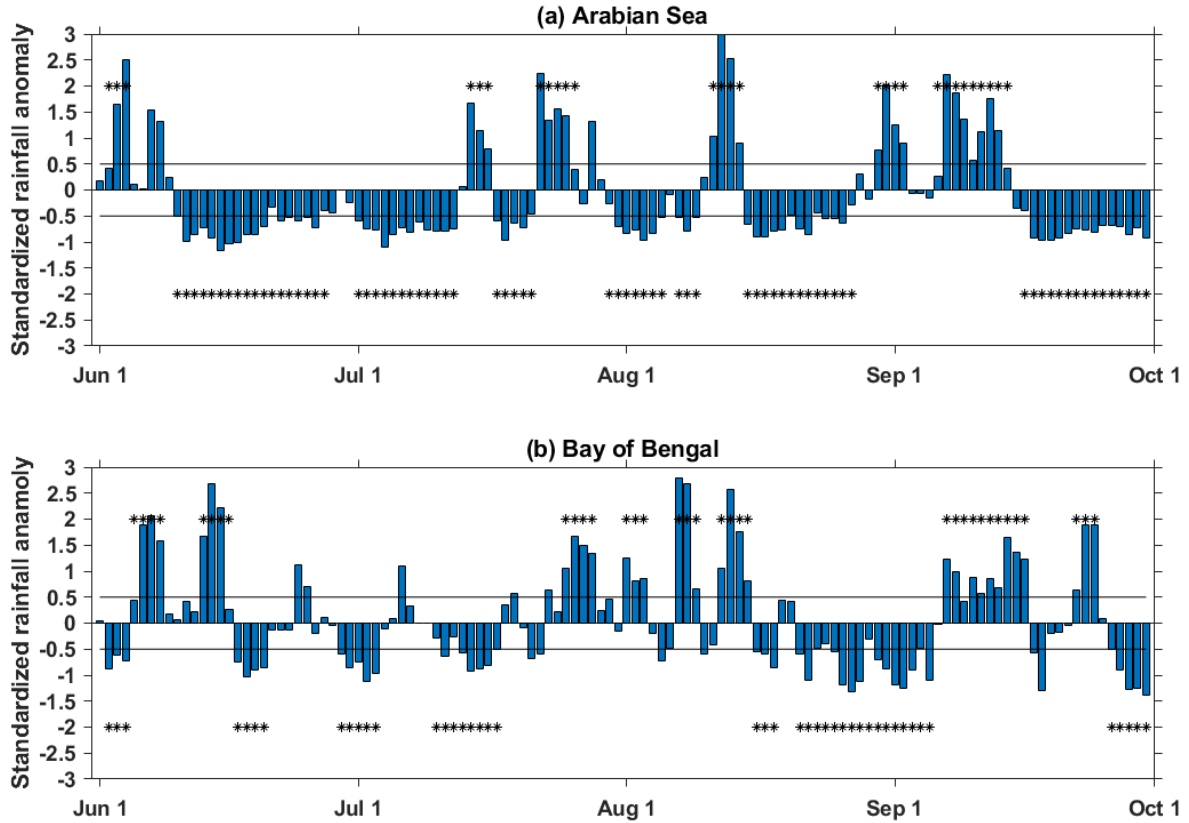
FIG. 8:(a) Time series of standardized rainfall anomaly during the SWM season for the year 2008 over the Arabian Sea (b) Same as (a) but for the Bay of Bengal. The

symbol (*) represents the active (on positive y - axis) and break spell days (on negative y − axis).

The typical example showing the identification of active and break spell days during the SWM for the year 2008 over AS and BOB are shown in FIG. 8. It is clear from the FIG. that over AS and BOB there are six and eight wet spells identified during SWM 2008 respectively. Whereas the dry spells are seven over both AS and BOB. In the similar fashion the wet and dry spell days are identified for both SWM and NEM over AS and BOB during 1998 to 2013.

Chapter 3

Intraseasonal variation of vertical structure of precipitation during SWM and NEM

3.1 Characteristics of wet and dry spells over AS and BOB
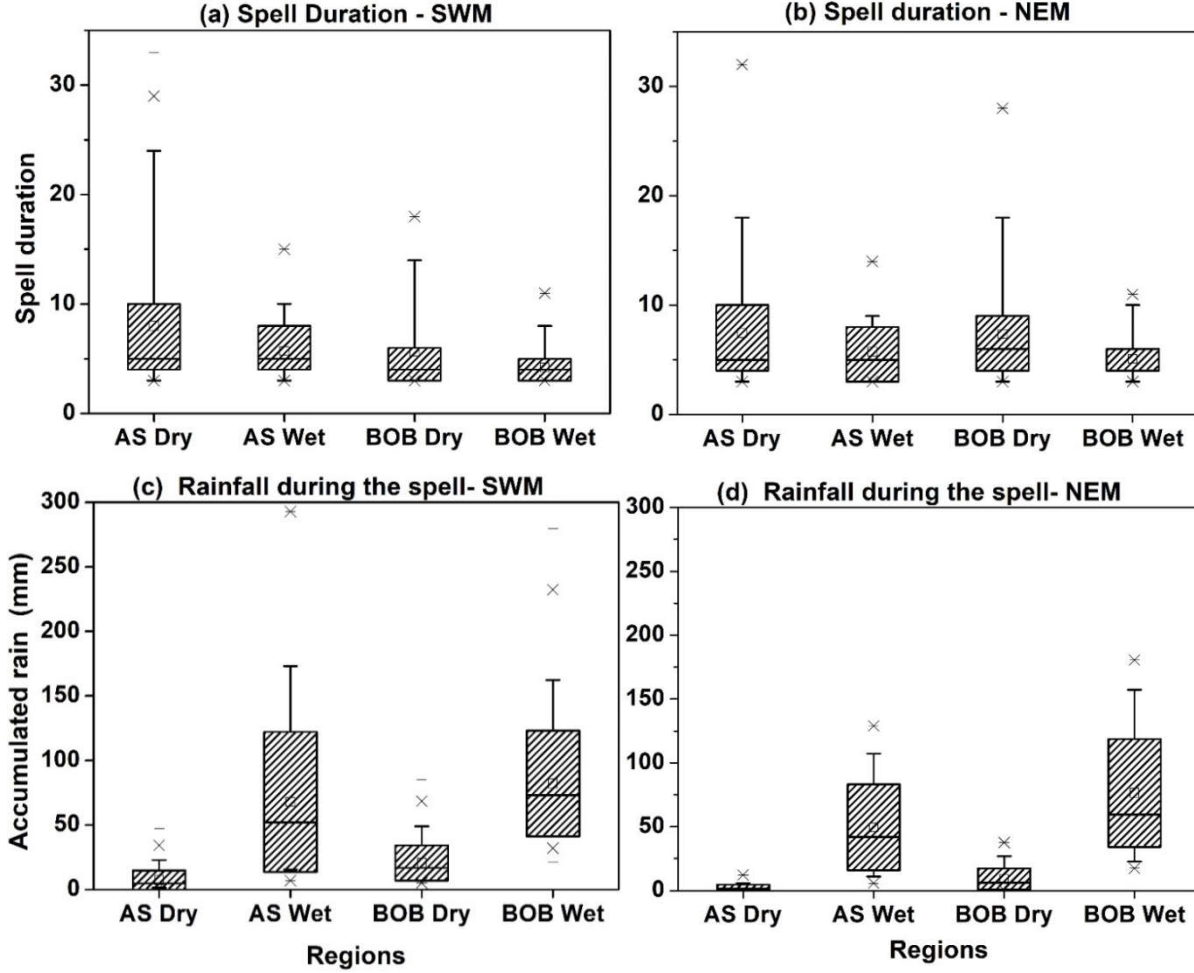
FIG. 9: (a) and (b) represents the distribution of duration of the spells in the wet and dry spells during the SWM and NEM season over the BOB and the AS respectively. (c) and (d) are same as (a) and (b), respectively, but for the accumulated rain during the spell.

The wet and dry spells are identified over AS and BOB during SWM and NEM for the period 1998-2013 by the method as mentioned in section 2.7. Box plots are constructed to compare the duration of the spell and the accumulated rainfall of the spell. The top and bottom edge of the each boxplot indicate the 25th and 75th percentile. The line in-between is the median, the small box inside is the mean. The whiskers represent the 5th and 95th percentile and the stars at the top and bottom represents the maximum and minimum values respectively (Fig. 9).The distributions of spell durations and accumulated rain over the AS and BOB of wet and dry spells during SWM and NEM are shown in FIG.9. Regardless of the season, the duration of the dry and wet spells is more over the AS than the respective spell over the BOB (Fig. 9a & 9b). However, contrary feature is observed in accumulated rain during the respective spells as evident from FIG. 9c & 9d. Even though the spell duration is less in BOB, the rainfall received during the respective spell is more when compared to the AS. The spell durations are similar for the dry spells of AS during

the SWM and NEM, but the duration is more in the NEM than in the SWM over BOB. However, the wet spell durations are same over the AS as well as over the BOB during the SWM and NEM. However, the durations are same during the SWM and NEM in the respective spells over AS, the accumulated rainfall is more in the SWM than in the NEM. Over BOB, the accumulated rainfall is same during the wet spells of SWM and NEM but in the dry spells, it is more in the SWM than in the NEM.

3.2 Variations in the occurrence and rain fraction of different rain types during wet and dry spells

The observed differences in the accumulated rainfall (Fig. 9c & 9d) could be due to the variations in the occurrence of convective, stratiform and shallow rain. Thus, the occurrence and rain fraction of convective, stratiform and shallow rain in the wet and dry spells during SWM and NEM over the AS and BOB are calculated and depicted in FIG. 10a & 10b. Rain fraction is the amount of rain contributed by a particular rain type to the total rain in a given spell and season. The occurrence of stratiform rain is more in the wet spells, whereas the occurrence of convective and shallow rain is more in the dry spells during both the seasons. The occurrence of stratiform and convective rain is more over the BOB than over the AS in both the spells. However, the shallow rain occurrence is more over the AS than over the BOB. As evidenced from FIG.10a & 10b, the increase in occurrence of shallow rain is prominent over the BOB during the dry spells from SWM (20%) to NEM (33%). Though the occurrence of convective rain is less, its contribution to the rain fraction is more than the other types of rainfall (except for shallow rain over the AS during the dry spell) during both the seasons. Similar to the occurrence, the rain fraction of convective and shallow rain (stratiform rain) is also more (less) in the dry spells than in the wet spells during both the seasons. To further examine these convective, stratiform and shallow rain are produced from which type of precipitating systems, the percentage occurrence of DCC, DWC, WCC, BSR and ISE during wet and dry spells over the AS and BOB are shown in FIG. 11. The occurrence and rain fraction of deeper precipitating systems (DCC, DWC, WCC and BSR) are more and isolated shallow systems are less in the BOB than in the AS during both the spells of SWM. While in the NEM, the occurrence and rain fraction of DCC, DWC and ISE is more and BSR is less over the AS than over the BOB. Regardless of the season and region, the occurrence and rain fraction of BSR and DWC are more and ISE are less during wet spells than the dry spells indicating the presence of large scale systems during wet spells and isolated shallow systems during the dry spells. Further, both occurrence and rain fraction of BSR and DWC are increasing and ISE are decreasing in dry spells from SWM to NEM over BOB. It is interesting to note that in both the spells, the occurrence and rain fraction of DWC are more over the BOB than over the AS during SWM while the contrary feature is evident during the NEM (Fig. 11).
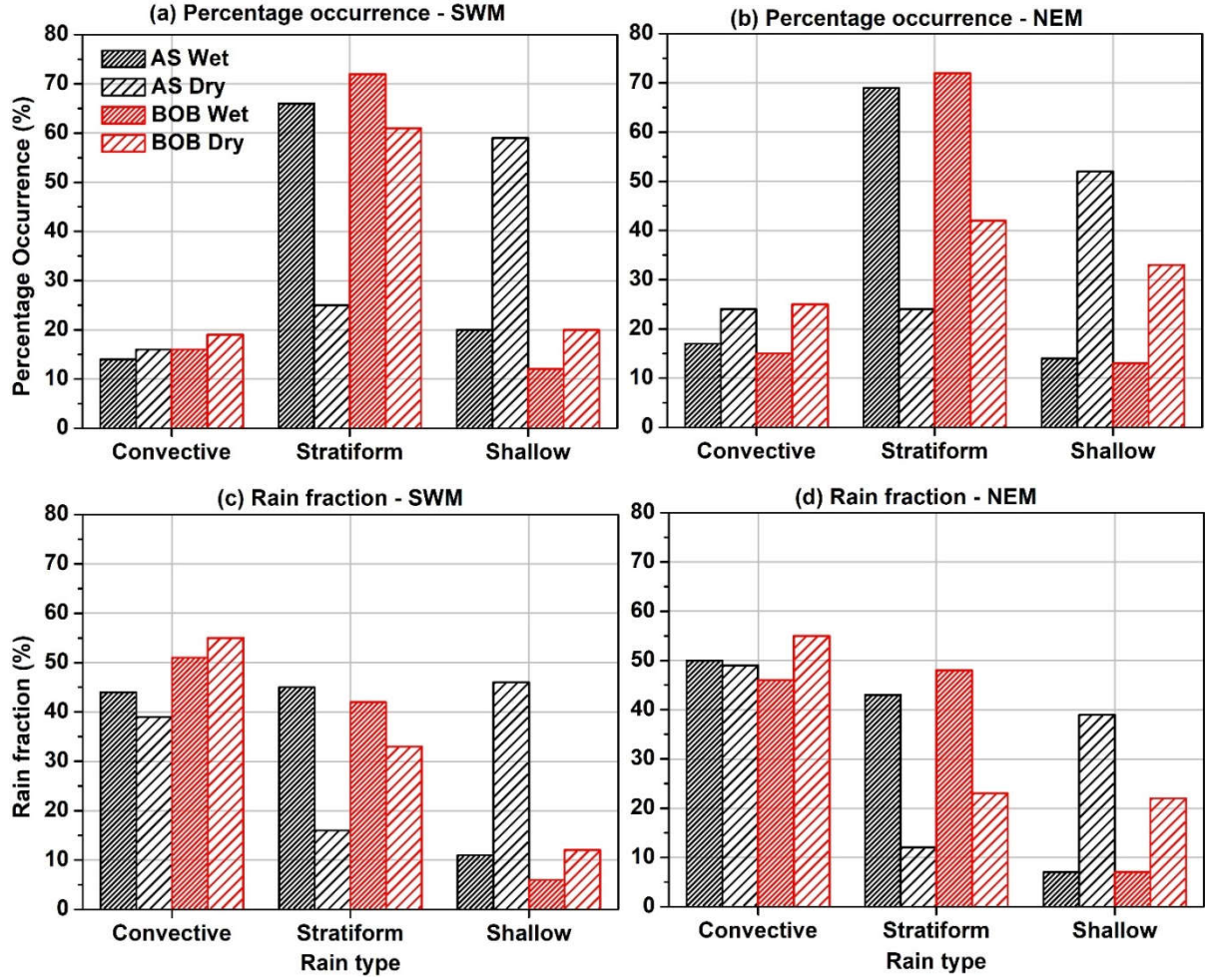
FIG. 10: (a) Occurrence of convective, stratiform and shallow rain in the wet and dry spells during the SWM season over the BOB and the AS. (b) Same as (a) but for NEM season. (c) and (d) are same as (a) and (b), respectively, but for the rainfraction.
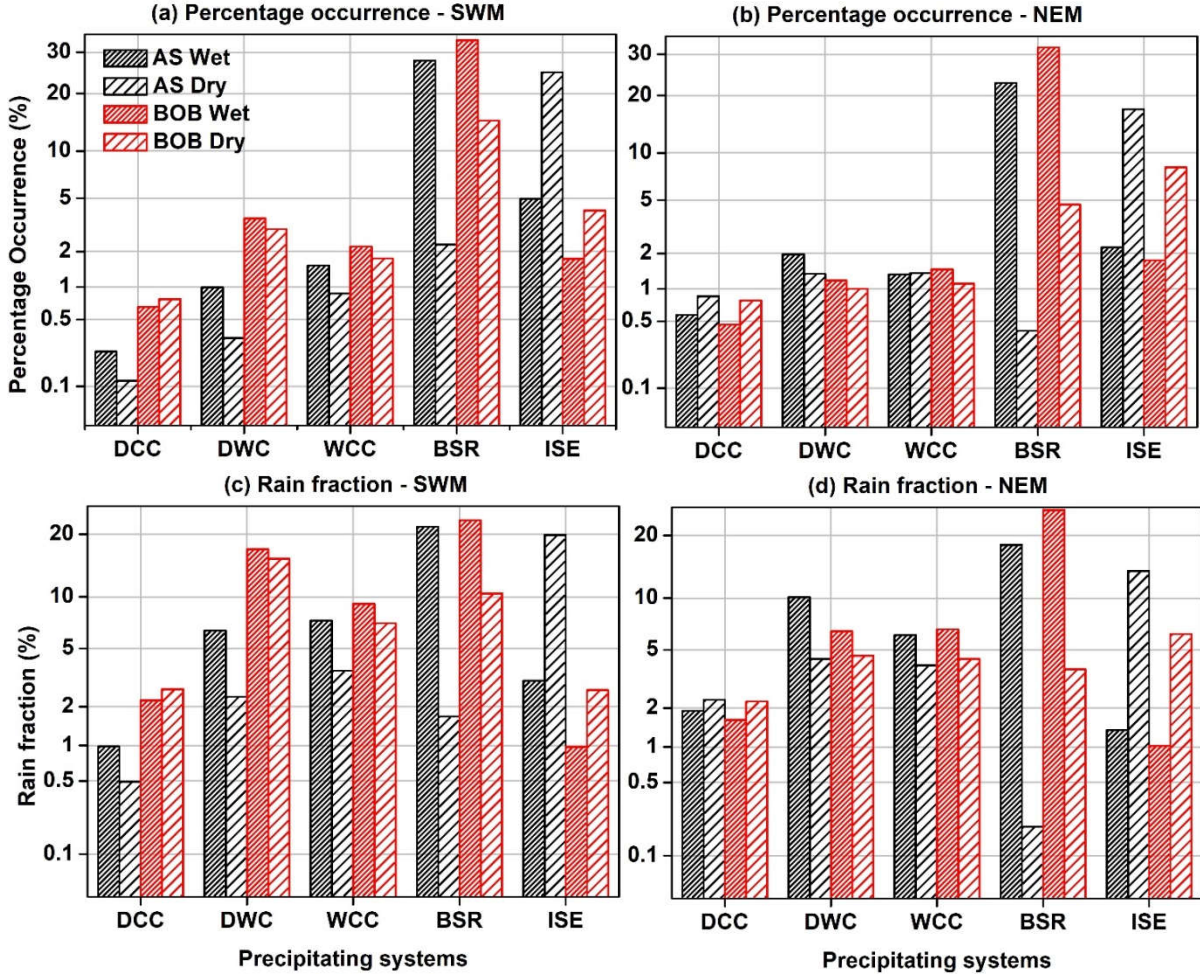
FIG. 11: (a) Occurrence of deep convective cores (DCC), deep wide convective cores (DWC), wide convective cores (WCC), broad stratiform regions (BSR), Isolated Shallow echoes (ISE) in the wet and dry spells during the SWM season over the BOB and the AS. (b) Same as (a) but for NEM season. (c) and (d) are same as (a) and (b), respectively, but for the rainfraction.

3.3 Differences in vertical structure of precipitation during wet and dry spells

To elucidate the vertical structure of precipitation in the wet and dry spells, the contour frequency by altitude diagrams (CFADs) of reflectivity (in dBZ) are constructed following [38]with a bin size of 1 dBZ reflectivity at each height interval over the AS and the BOB during the SWM and NEM and are depicted in FIG. 12. The CFADs are constructed in such a way that the count at each reflectivity bin of each height interval is normalized by the maximum value (the maximum value out of all the reflectivity bins at all the heights) and multiplied by 100. Hence the CFADs represent the the percentage of occurrence w.r.t maximum value. The large occurrence of reflectivity below 4 km altitude in the dry spells over the AS during both the seasons and dry spells of BOB during NEM indicates the prevalence of shallow rain in those spells (also seen in FIG.10 and 11). On the other hand except in the dry spell of SWM over the AS, reflectivity distribution shows predominance of deep (convective and stratiform) rain. Irrespective of the spells, the

occurrence of shallow rain is copious over the AS during the SWM. The reflectivity distributions in the respective spells below 4 km altitude show larger values in the NEM than in the SWM. This implies that in a given spell, the occurrence of shallow rain is larger in NEM than in SWM (Figs. 10a-b& 11a-b).The CFADs of reflectivity also show broader distributions in the wet spells than the dry spells during both the seasons. The median reflectivity profiles (Fig. 12e &12j) are same for the wet spells as well as for the dry spells over both the seas during the NEM. However, below the melting layer the median reflectivity values are larger in the dry spells over the BOB than the AS and are nearly the same in the wet spells. Irrespective of the season, the precipitating systems penetrate to deeper heights in the wet spells than in the dry spells.

To further study about the storm heights, the distributions of storm heights (the topmost height of the reflectivity profile with three consecutive lower range bins having conditional reflectivity values ≥ 17 dBZ; [23, 38]) are computed in the wet and dry spells of SWM and NEM and are depicted in FIG.13. The storm height distributions are distinctly different for dry and wet spells over the AS during both the seasons. However, the distributions are identical over the BOB during the SWM and show large variations during the NEM. The occurrence of deep systems decreases and shallow systems increases substantially during the dry spells of NEM over the BOB, which results in a pronounced peak at 3km (Fig. 13b). The storm height peak observed at 3 km altitude over the AS during SWM and over both the seas in the dry spells of NEM also confirms the predominance of shallow rain in those spells. Nevertheless, the other peak seen at ˜6 km altitude is due to stratiform rain occurrence with feeble echoes at the upper heights for which TRMM-PR is not sensitive [23]. The storm height distributions show bimodality over BOB in the dry spells of NEM. The storm height distributions confirm that the deep systems occurrence is more in the wet spells than in the dry spells over both the seas. Irrespective of the spell, the occurrence of deep systems is more and shallow systems is less over the BOB than over the AS.
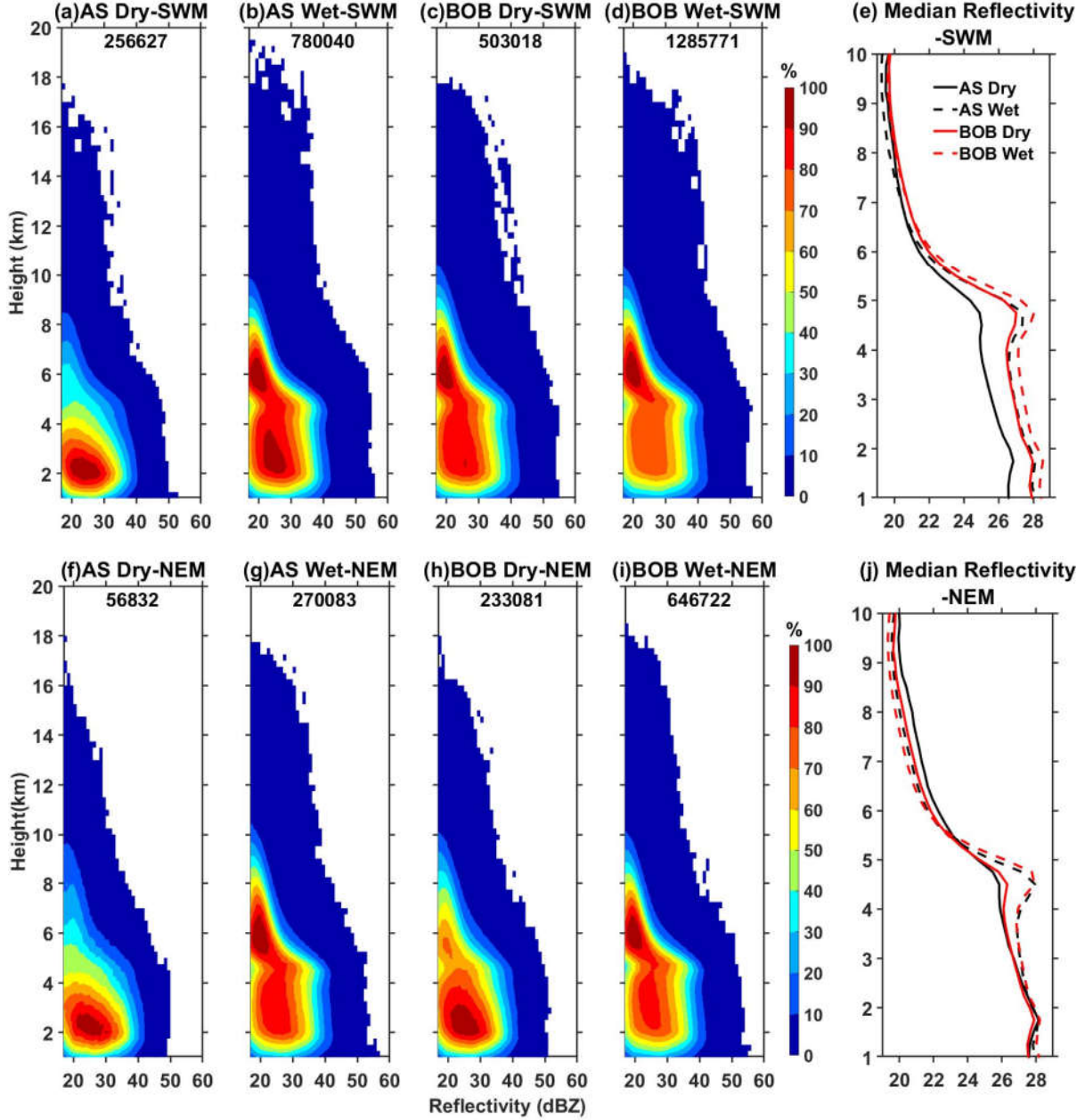
FIG. 12: (a) and (c) are the CFADs of reflectivity (dBZ) in the dry periods over the AS and the BOB, respectively, during the SWM season. (b), and (d) are same as (a) and (c) but for wet periods. (f), (g), (h) and (i) are same as (a), (b), (c) and (d),respectively, but for NEM season. (e) and (j) represents the median reflectivity profile during SWM and NEM respectively.
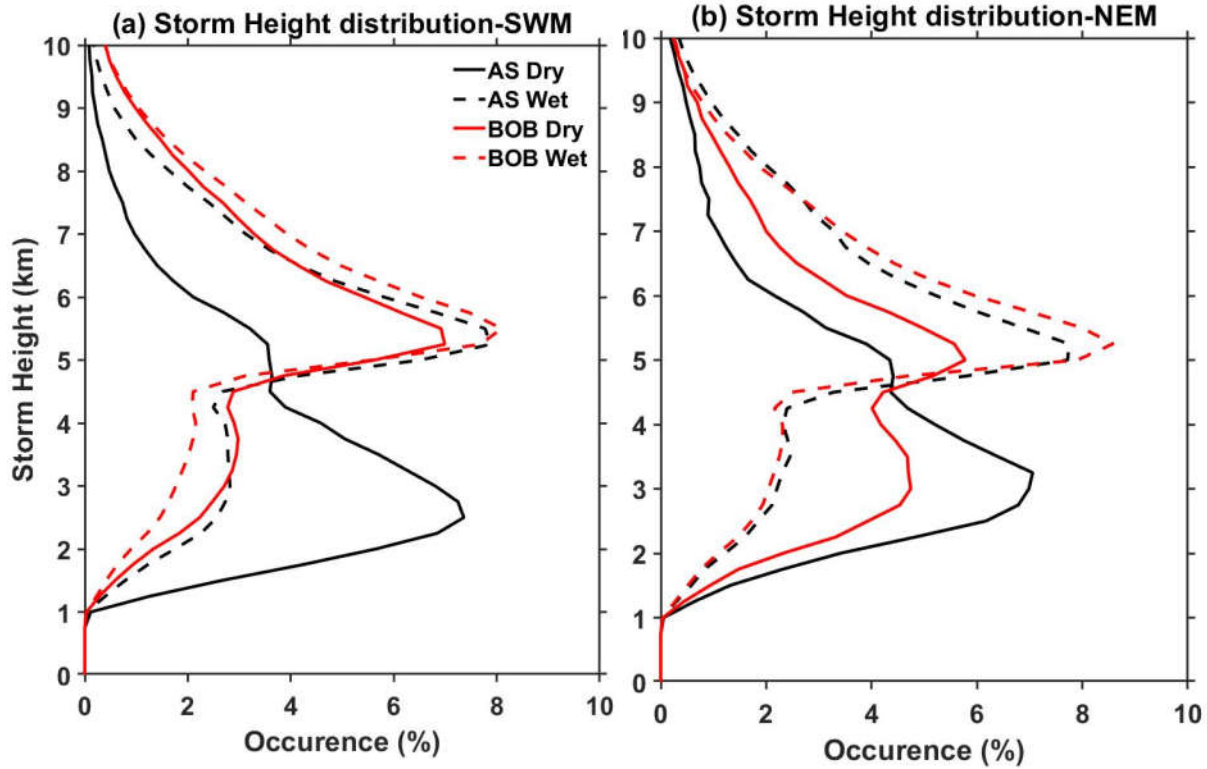
FIG. 13: (a) Distribution of conditional reflectivity (17 dBZ) echo top altitude with height in the wet and dry periods during the SWM over the AS and the BOB. (b) Same as (a) but during the NEM season.

3.4 Background atmospheric conditions in the dry and wet spells

The variations observed in the occurrence of different kinds of precipitating systems during the dry and wet spells of SWM and NEM over the AS and BOB could be due to the differences in surface forcing (sea surface temperature) and/or the background atmospheric conditions [29, 30, 39]. In order to check the role of surface forcing on the occurrence of various kinds of precipitating systems, the distributions of sea surface temperature (SST) in wet and dry spells of SWM and NEM over the AS and BOB are plotted in FIG. 14. The SST distributions are identical in the dry and wet spells of BOB during both the seasons, while the occurrence of larger SSTs are more and smaller SSTs are less in the wet spells than in the dry spells over the AS during SWM. On the other hand, the distributions are similar for dry and wet spells over the AS during the NEM. Regardless of the spells and seasons, SSTs are larger over the BOB than over the AS. This indicates that the surface forcing is larger over the BOB than over the AS in both the monsoon seasons. Inter comparison of spells show same surface forcing in dry and wet spells over the BOB and show smaller values in the dry spells than in wet spells over the AS during the SWM. On the other hand, the surface forcing is same for the dry and wet spells over both the AS and BOB during the NEM.

FIG. 14: (a) Distribution of SST (°C) in the wet and dry periods during the SWM over the AS and the BOB. (b) Same as (a) but during the NEM season.

Precipitating system size and vertical extent depends not only on the surface forcing but also on the background atmospheric conditions [39] like the total column water vapour (TCWV), equivalent potential temperature (θ_e), relative humidity and vertical velocity. The distributions of TCWV during dry and wet spells of SWM and NEM are plotted in FIG.15. Overall, the TCWV values are larger in the wet spells than in the dry spells over both the seas and seasons. During SWM, TCWV distributions are alike over the AS and the BOB in the wet spells and possess larger values over the BOB than the AS in the dry spells. TCWV values are larger in both the dry and wet spells over the BOB than over the AS during NEM.
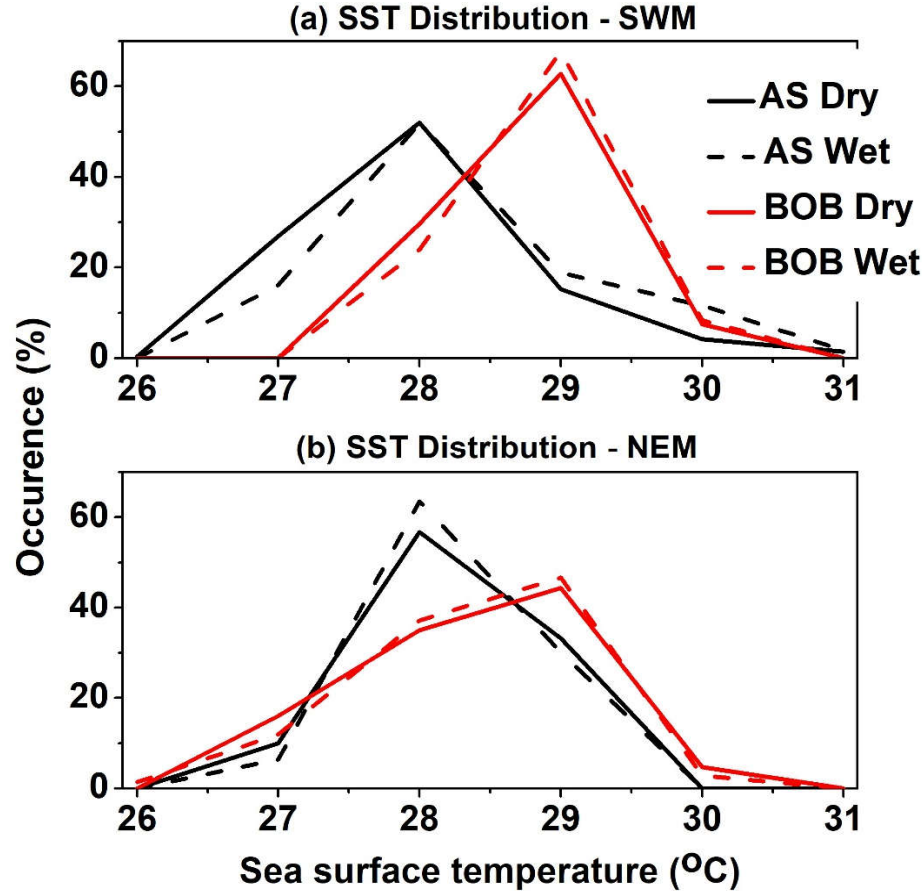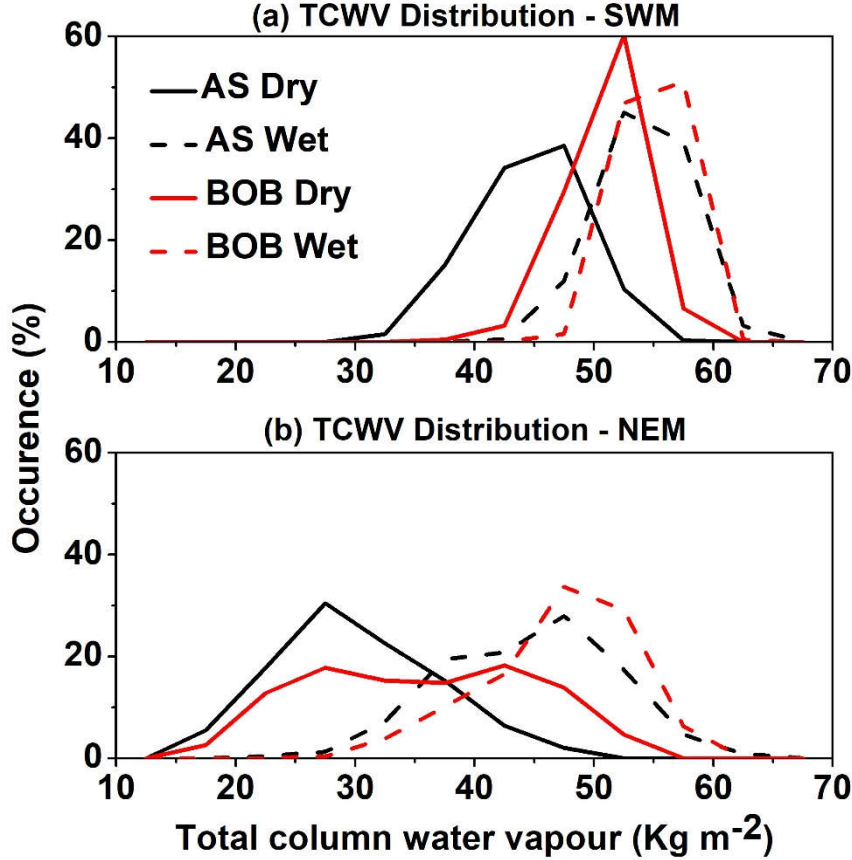
FIG. 15: (a) Distribution of TCWV (kg m^{-2}) in the wet and dry periods during the SWM over the AS and the BOB. (b) Same as (a) but during the NEM season.

To know the stability of the air parcel at different altitudes the mean vertical profiles of θ_e, for the available moisture mean profiles of relative humidity (RH) and for the dynamical effects the mean profiles of vertical wind are computed in the respective spells and seasons and are plotted in FIG.16. The surface θ_e is same for wet and dry spells over the AS and BOB however, the values are larger over the BOB than over the AS during the SWM. Irrespective of the spell and region, the surface θ_e is same during the NEM. The gradients of θ_e clearly show (Fig. 16a) the presence of stable layers between 900 and 800 hPa levels in the dry spells over the AS and such stable layers are absent in the wet spells during the SWM. These stable layers are not persisting over the BOB (Fig. 16a & 16b) during both the seasons and over the AS during the NEM (Fig. 16b). The vertical distribution of RH depicts distinctly different features in the dry and wet spells during both the seasons (Fig. 16c & 16d). The lower- and mid-troposphere are relatively drier in the dry spells than in the wet spells. Regardless of the spell, the relative humidity is larger over the BOB than over the AS. The mid troposphere is driest over the AS during SWM and over both the regions during NEM. The mean vertical wind depicted in FIGs. 16e & 16f shows an upward wind during the wet spells. In dry spells, a downward motion is apparent in the middle troposphere over the AS and an upward motion persists at all levels in both the regions during the SWM. However, a downward motion during

27

the dry spells and upward motion during the wet spells is observed at all levels in the NEM. The strength of upward motion is larger during the wet spells and downward motion is smaller during the dry spells over the BOB than over the AS.

3.4.1 Dry Spells over the AS

The dry spells of AS during SWM have less surface forcing, low TCWV values, strong inversion layers below 800 hPa level, dry mid-troposphere and downward vertical wind in the mid-troposphere during the SWM. However, the NEM dry spells have less surface forcing, lowest TCWV values, driest mid-troposphere and prevailing downward vertical wind across all the heights. As shown in [39], in the presence of less surfacing forcing and low TCWV values small scale systems will be formed. These systems vertical growth is strongly retarded by the inversion layers and downward motion and hence precipitates in the form of shallow rain. Thus, the occurrence of shallow rain is dominant in both the seasons over the AS. As the inversion layers are nearly absent during the NEM, the shallow rain occurrence is relatively less in the NEM than the SWM. The less occurrence of stratiform rain also confirms the presence of more small scale systems in the dry spells, which is in accordance with the findings of [39]. As shown in [26, 30] the occurrence of shallow systems decreases and deep systems increases with increase in SST. As SST increases the surface forcing increases, TCWV increases, the occurrence of inversion layers decreases and mid-troposphere becomes moisten which favors the vertical and horizontal growth of precipitating systems [26, 29].Therefore, the deep convective and stratiform rain occurrence is possible at SSTs greater than 28°C.

3.4.2 Wet Spells over the AS

The wet spells of AS during SWM possess larger SSTs indicating enormous surface forcing, larger TCWV values, moist troposphere and upward vertical wind than the dry spells. Also, the temperature inversions present in the dry spells are nearly absent in the wet spell conditions. Nonetheless, the NEM have approximately same surface forcing, larger TCWV values, moist troposphere, and upwards vertical wind than the dry spells. The moist mid troposphere, larger TCWV values and upward motion favors the growth of precipitating systems both in horizontal and vertical dimensions and produce large scale systems. This is evidenced from the considerable increase in the occurrence of stratiform (~5%) rain and decrease in the occurrence of shallow (~8 %) rain than the respective dry spells.

3.4.3 Dry spells over the BOB

The dry spells of SWM over BOB show large surface forcing, moderate TCWV, moist mid-troposphere and weak upward vertical wind at all the levels. However, the NEM also show large surface forcing, weak to moderate TCWV, dry mid-troposphere and weak downward vertical wind at all the levels. The temperature inversions are almost absent in the lower troposphere in both the seasons. Large surface forcing and moderate TCWV values favors the formation of large scale systems however the moist mid troposphere and upward vertical winds allow the systems to grow to deeper heights in SWM and the dry mid-troposphere and downward vertical wind inhibits the vertical growth in NEM. This

result in relatively more occurrence of stratiform rain (~18%) and less occurrence of shallow rain (~13%) in the SWM than in the NEM as evidenced from FIG. 10.

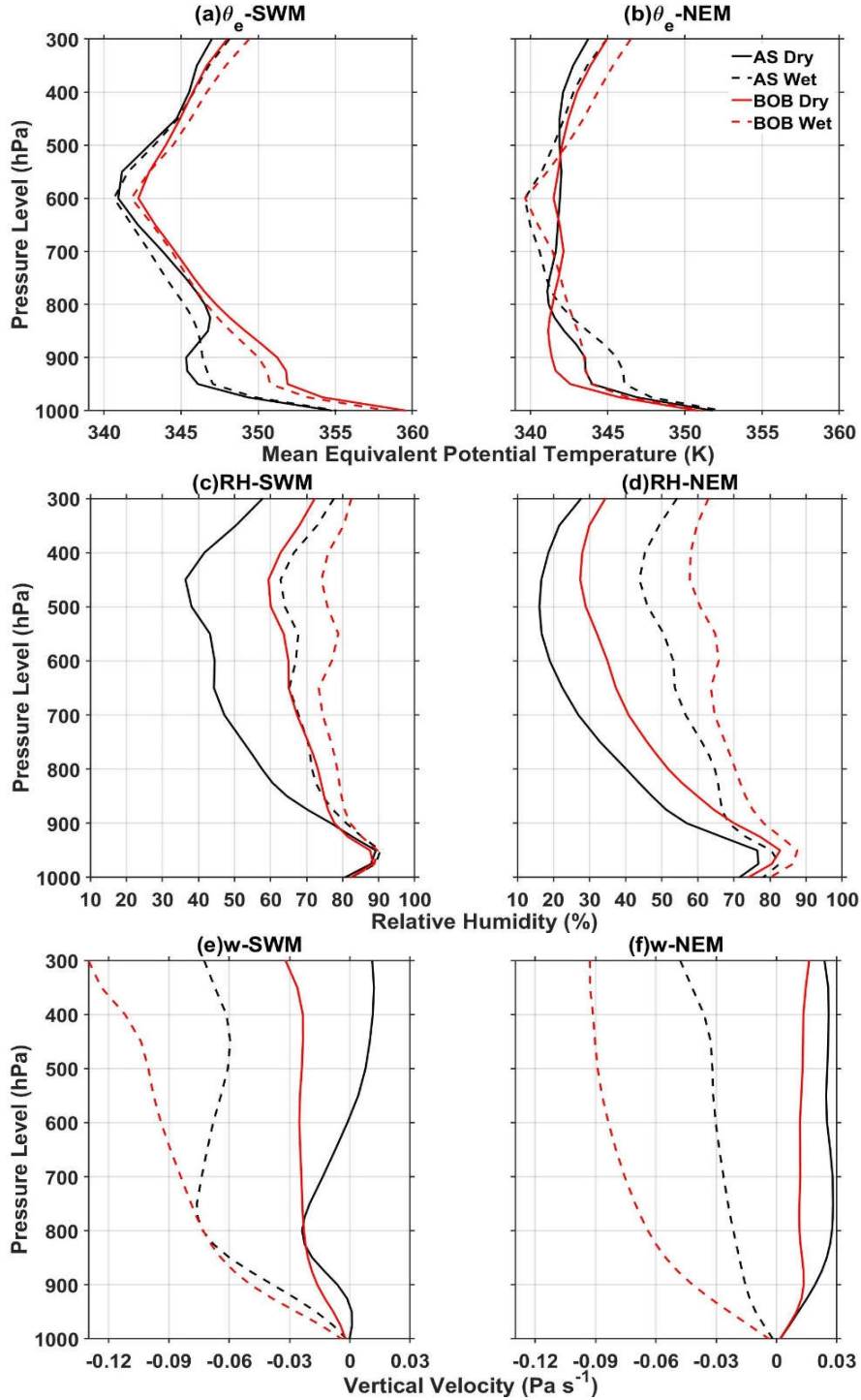**FIG. 16:** (a) Vertical profiles of mean θ_e (°K) in the wet and dry periods during the SWM over the AS and the BOB. (b) Same as (a) but during the NEM season. (c) and

(d) are same as (a) and (b) respectively but for RH (%). (e) and (f) are same as (a) and (b) respectively but for vertical wind (Pa s^{-1}).

Intercomparison of atmospheric parameters over the AS and BOB reveals that the dry spells of BOB show larger TCWV values, more moisture in mid-troposphere, weaker upward motion instead downward motion in the mid-troposphere and nearly no inversions in the lower troposphere than the AS. Hence, the occurrence of stratiform rain is more (~36% in SWM & ~17% in NEM) and shallow rain is less (~39% in SWM & ~19% in NEM) over the BOB than over the AS.

3.4.4 Wet Spells over the BOB

BOB wet spells during both the seasons possess large surface forcing, largest TCWV values, moist mid-troposphere, strong upward vertical wind and no inversions layers in the lower troposphere. All these atmospheric conditions favor the formation of large scale systems that results in larger occurrence of stratiform rain and lesser occurrence of shallow rain as evidenced in FIG. 10. Since, the background atmospheric conditions are similar in both the seasons the occurrence of different kinds of rainfall (convective, stratiform and shallow) are also same during the wet spells. As evidenced from FIG. 3, the surface forcing differs slightly from SWM to NEM but similar for the dry and wet episodes in each season. Hence, the differences observed between dry and wet spells are due to background atmospheric parameters over the BOB. The arid mid-troposphere in the dry spells of NEM is the major cause for the observed large occurrence of shallow rain, which is not frequent over the BOB.

Chapter 4

Summary and future work

4.1 Summary

4.2 Future scope of the thesis

4.1. Summary:

TRMM-PR (1998-2013) augmented with ERA5 reanalysis dataset are used to study the variation of rain types, vertical structure of precipitation and their associated background environmental conditions over AS and BOB during the wet and dry spells of SWM and NEM. Irrespective of the season, substantial differences are observed in the occurrence, rain fraction and vertical structure of precipitation due to varying background atmospheric parameters during the wet and dry spells of SWM and NEM. This analysis reveals the following:

- Regardless of the spell, the occurrence and rain fraction of deep systems (DCC, WCC, DWC, and BSR) are more and shallow systems are less in BOB than AS during the SWM.

- The occurrence of shallow systems is plentiful in dry spells of AS during both the seasons. In concurrence with this, the storm height and reflectivity distribution also shows the higher occurrence around 3km altitude. During the dry spells of AS, the observed driest mid troposphere, lowest TCWV, downdrafts in the lower and mid-troposphere and presence of stable layers in lower troposphere retard the vertical growth of precipitating systems that results in isolated shallow systems.

- In the dry spells of BOB, both rain fraction and occurrence of stratiform and convective (DWC) rain decreases whereas the occurrence of shallow systems increases from SWM to NEM. The increase in the shallow systems results in bimodal distribution (around 3km and 5.5km) in both storm height and reflectivity distributions. The observed drier mid-troposphere, more stable layers in lower troposphere, lesser TCWV and strong downdrafts in the NEM than in the SWM results in higher occurrence of shallow systems than the deep systems during the NEM.

- During the wet spells, the changes in the occurrence and rain fraction of different rain types are marginal in both the seasons and seas. The prevalence of deeper systems than the shallow systems is due to changes in background atmospheric conditions from dry spells to wet spells. Compared to the dry spells, the moist mid-troposphere, updrafts in the lower and middle troposphere, the absence of lower tropospheric stable layers and higher TCWV favour the vertical growth of precipitating systems that result in occurrence of more deeper systems during the wet spells of both the seasons.

4.2. Future scope of the thesis:

The climatological variation of precipitating systems there vertical structure during wet and dry spells are studied in this work. However the rainfall variations during the inter annual weather events like El Nino and La Nina effects the rainfall over India and surrounding seas at seasonal scales are documented. Nevertheless, the variation of rainfall during El Nino and La Nina in wet and dry spells over the Indian Ocean are less known. The present study motivates to understand the variation of rainfall during the wet and dry spells in such events. This kind of understanding of the precipitating systems are different temporal scales is significant for the better prediction of rainfall in the models.

Bibliography

[1] S. Gadgil, Annu. Rev. Earth Planet. Sci. **31**, 429–467 (2003).

[2] M. Rajeevan, C. Unnikrishnan, J. Bhate, K. Niranjan Kumar, and P. Sreekala, Meteorol. Appl. **19(2)**, 226–236 (2012).

[3] P. Mukhopadhyay, S. Taraphdar, B. N. Goswami, and K. Krishnakumar, Wea. Forecasting. **25**, 369–387(2010).

[4] C. T. Sabeerali, A. Ramu Dandi, A. Dhakate, K. Salunke, S. Mahapatra, and S. A. Rao, J. Geophys. Res. Atmos. **118**, 4401–4420 (2013).

[5] R. S. Ajayamohan, B. Khouider, A. J. Majda, and Q. Deng, Clim. Dyn. **47**, 3641–3660 (2016).

[6] P. J. Webster, V. O. Magana, T. N. Palmer, J. Shukla, R.A. Tomas, M. Yanai, and T. Yasunari, J. Geophys. Res. Atmos. **103**, 14451–14510 (1998).

[7] V. Krishnamurthy, and B. N. Goswami, J. Climate. **13**, 579–595 (2000).

[8] B. N. Goswami, G. Wu, and T. Yasunari, J. Climate. **19**, 5078–5099 (2006).

[9] E. Suhas, J. Neena, and B. N. Goswami, J. Atmos. Sci. **69**, 1761– 1774 (2012).

[10] M. Rajeevan, S. Gadgil, and J. Bhate, J. Earth Syst. Sci. 119: 229– 247 (2010).

[11] B. Radhakrishna, T. N. Rao, and K. Saikranthi, J. Hydrometeorol. **20**, 45–58 (2019).

[12] R. Chattopadhyay, B. N. Goswami, A. K. Sahai, and K. Fraedrich, J. Geophys. Res. Atmos. **114**, D19114, (2009).

[13] A. Pathak, S. Ghosh, P. Kumar, and R. Murtugudde, Sci. Rep. **7**, 12729 (2017).

[14] N. Karmakar, and T. N. Krishnamurti, Clim. Dyn.**52(3)**, 1903–1916 (2019).

[15] R. Krishnan, C. Zhang, and M. Sugi, J. Atmos. Sci. **57(9)**, 1354–1372 (2000).

[16] N. Karmakar, A. Chakraborty, and R. S. Nanjundiah, Mon. Weather Rev. **145(2)**, 413–435 (2017).

[17] N. Karmakar, and V. Misra, J. Geophys. Res. Atmos. **125**, e2019JD031648 (2020).

[18] A. K. Rowe, R. A. Houze, S. Brodzik, and M.D. Zuluaga, J. Atmos. Sci. **76**, 1975-1988 (2019).

[19] S. Shige, Y. N. Takayabu, W. K. Tao,and D. E. Johnson, J. Appl. Meteorol. **43**, 1095–1113 (2004).

[20] W. Tao et al, B. Am. Meteorol. Soc. **87**, 1555–1572 (2006).

[21] U. Romatschke, S. Medina, and R. A. Houze, J. Climate. **23**, 419–439 (2010).

[22] U. Romatschke, and R. A. Houze, J. Hydrometeorol. **12**, 3–26 (2011).

[23] K. Saikranthi, T. N. Rao, B. Radhakrishna, and S. V. B Rao, J. Geophys. Res. Atmos. **119**, 8433–8449 (2014).

[24] G. S. Bhat, and S.S. Kumar, J. Geophys. Res. Atmos. **120**, 1710–1722 (2015).

[25] J. Phadtare, and G. S. Bhat, Mon. Weather Rev. **147**, 3741-3758 (2019).

[26] K. Saikranthi, B. Radhakrishna, S. K. Satheesh, and T. N. Rao, Clim. Dyn. **50**, 3671–3685 (2018).

[27] A. K. M. Nair, and K. Rajeev, J. Climate. **27**, 672–683 (2014).

[28] S. Gadgil, P. V. Joseph, and N. V. Joshi, Nature. **312**, 141–143 (1984).

[29] K. Saikranthi, B. Radhakrishna, T. Narayana Rao, and S. K. Satheesh, Int. J. Climatol. **39(11)**, 4305-4312 (2019a).

[30] K. Saikranthi, B. Radhakrishna, T. Narayana Rao, and S. K. Satheesh, Atmos. Chem. Phys. **19**, 10423–10432 (2019b).

[31] J. Awaka, T. Iguchi, and K. Okamoto, J. Meteorol. Soc. Jpn. **87a**, 31–52 (2009).

[32] R. A. Houze Jr., D.C. Wilton, and B. F Smull, Quart. J. Roy. Meteor. Soc. **133,** 1389-1411 (2007).

[33] Copernicus Climate Change Service (C3S) (2017): ERA5: Fifth generation of ECMWF atmospheric reanalyses of the global climate. Copernicus Climate Change Service Climate Data Store (CDS), date of access. https://cds.climate.copernicus.eu/cdsapp#!/home

[34] J. M. Wallace, and P. V Hobbs, *Atmospheric science: An introductory survey, (*Academic press, 2006) Edition 2, p.85

[35] R. W. Reynolds, T. M. Smith, C. Liu, D. B. Chelton, K. S. Casey, and M. G. Schlax, J. Climate. **20**, 5473-5496 (2007).

[36] P. Singh, and K. Nakamura, J. Geophys. Res. **115**, D12122, (2010).

[37] D. Shrestha, P. Singh, and K. Nakamura, J. Geophys. Res. **117**, D22106 (2012).

[38] T. N. Rao, K. Saikranthi, B. Radhakrishna, and S. V. B. Rao, J. Climate. 29, 7797-7814 (2016).

[39] Q. Chen, J. Fan, S. Hagos, W. I. Gustafson Jr, and L. K. Berg, J. Geophys. Res. Atmos. **120**, 6551–6574 (2015).

[40] C. Schumacher, R. A. Houze, and I. Kraucunas, J. Atmos. Sci., **61**, 1341–1358(2004).

[41] C. Donald Ahrens, *Essentials of Meterology: An invitation to the Atmosphere* (Brooks Cole, 2010). Edition 6.

[42] TRMM Precipitation Radar Team (JAXA and NASA collaboration), *TRMM Precipitation Radar Algorithm Instruction Manual* (2011) Version 7.